Hydrate Stability of Carbon Dioxide + Oxygen Binary Mixture (CO 2 + O 2) in Pure Water: Measurements and Modeling

Salaheddine Chabab, Alain Valtz, Snaide Ahamada, Christophe Coquelet

Hydrate Stability of carbon dioxide + oxygen binary mixture ($CO_2 + O_2$) in pure water: Measurements and modeling

Salaheddine Chabab[a], Alain Valtz[a], Snaide Ahamada[a], Christophe Coquelet[a,*]

[a]*Mines ParisTech, PSL University, CTP-Centre of Thermodynamics of Processes, 35 rue Saint Honoré, 77305 Fontainebleau Cedex, France*

*Corresponding author. Tel: +33164694962, E-mail address: christophe.coquelet@mines-paristech.fr (C. Coquelet)

Abstract

Knowledge of the dissociation conditions of mixed-gas hydrate systems is of great importance for scientific understanding (e.g. Clathrate hydrates in the outer solar system) and engineering applications (e.g. flow assurance, refrigeration and separation processes). In this work, CO_2+O_2 hydrate dissociation points were measured at different O_2 mole fractions (11%, 32% and 50%) using isochoric pressure search method. The consistency of these new data was verified using the Clausius-Clapeyron relationship. The measurements performed for pressures up to 19 MPa overcome the lack of data for this system, and also allows to evaluate the model predictions from pure CO_2 hydrate to pure O_2 hydrate. To predict gas hydrate stability curves, in this work, the well-established hydrate theory of van der Waals and Platteeuw (vdWP) is combined with an electrolyte CPA-type Equation of State (e-PR-CPA EoS) which has been successfully used to represent with high accuracy the fluid phase equilibria (including gas solubility and water content) of complex systems containing gas, water and salt. The resulting model (e-PR-CPA + vdWP) was applied to the O_2+H_2O and CO_2+H_2O+(NaCl) systems by comparing with literature data. In the studied temperature range (>270K), the model predicts as expected a hydrate structure of type I for O_2, CO_2 and their mixtures. An excellent reproduction of the measured data by this complete model was obtained without any additional adjustable parameters.

1. Introduction

The growing integration of renewable energies, mainly intermittent (with issues of overcapacity and redundancy) in the short term (energy transition) and the total replacement of fossil hydrocarbons use in the long term, requires a flexible solution for large-scale energy storage. In the framework of the ANR (Agence Nationale de la Recherche) FLUIDSTORY project, a combination of Power-to-Gas (PtG) and Gas-to-Power (GtP) technologies with temporary underground gas storage is proposed as a solution for storing intermittent surplus renewable electricity while recovering and keeping CO_2 in a closed loop. To manage the temporal differences between the gas production from PtG and the gas consumption (GtP), this concept called EMO (Electrolysis-Methanation-Oxycombustion) involves the underground storage of these different energy carriers (O_2, H_2, CH_4, CO_2) in salt caverns built in very tight salt layers, with very large volumes, and which can withstand very high pressures (that can exceed 200 bars depending on the depth of the reservoir). Under certain temperature and pressure conditions (especially at temperatures below the critical temperature of CO_2 and at high pressure), CO_2 can be stable in the liquid state, which is not desired in underground storage because of the thermal effects on the rock (the salt layer) due to the phase transitions that the gas undergoes. The proposed solution is the storage of CO_2 and O_2 in the same cavern. The mixing of the two gases reduces the critical temperature of the mixture (CO_2+O_2) and keeps the gas in a supercritical state under the operating conditions of the storage. However, for the design and simulation of storage facilities and also for the evaluation of possible risks, it is necessary to study the thermophysical properties of this mixture.

In some cases, the temperature in the storage reservoir may be low enough to form hydrates in the wellhead or in surface facilities (pipes, compressors, etc.) [1, 2]. The large temperature difference between the bottom of the reservoir and the wellhead is due to the thermal gradient that depends on the depth and nature of the geological formation and also due to the Joule-Thomson effect resulting from the rapid expansion (high flow rate) of the extracted gas. Kleinitz and Boehling [3] presented temperatures of some underground storage facilities showing the necessity of injecting hydrate inhibitors in the reservoir to avoid blockage of the flow path and possibly the stoppage of production for maintenance purposes. To limit these flow assurance issues, it is crucial to know the temperature and pressure conditions under which gas hydrates are stable. In addition, important properties to be studied for such storage applications include the gas density and viscosity, its solubility in brine, as well as gas hydrate stability curves. In our recent work, we have studied the density of the CO_2+O_2 mixture [4] and

the solubility of CO_2 [5, 6], O_2 [6] and H_2 [7] in brine under underground storage conditions. Herein, in the continuity of the previous work, we are interested in the study of the dissociation points of the hydrates of CO_2, O_2 and their mixtures under the transport and storage conditions. Generally thermodynamic models are parameterized only on binary systems by optimizing binary interaction parameters, and therefore thanks to mixing rules, phase equilibria (fluid-fluid and hydrate-fluid) of multi-component (more than two compounds) systems can be predicted. This reduces the number of experiments required. However, a minimum of measurements must be performed to validate model predictions.

Several studies have reported dissociation point data for CO_2 and O_2 hydrates. However, to date there are no published data on the hydrates of the mixture of these two gases (CO_2+O_2). Chapoy et al. [8] measured and modelled a representative CO_2-rich flue gas system in the presence of impurities (O_2, Ar and N_2). This study and other ones [9, 10] showed that even in small concentrations, the presence of these impurities changes the phase diagram of the system. In a Joint Industry Project (JIP) report on the impact of impurities on the CCS chain, Chapoy et al. [11] also reported four measurement points of hydrate dissociation of the CO_2+O_2 mixture (5mol% of O_2). The present work aims to complete this study by measuring and modelling the CO_2+O_2 system at different compositions (especially for compositions above 5% of O_2). The new data measured in the context of the transport and storage of CO_2 and O_2 containing streams can also be used for other applications, for instance: 1) hydrate separation processes, in particular CO_2 capture from oxy-combustion flue gas [12] which mainly contain CO_2, O_2 and H_2O by gas hydrates formation since CO_2 hydrates are more stable than other gas hydrates (flue gas impurities) [13]; 2) the study of mixed gas hydrates in the outer solar system [14]; 3) and finally allowing the evaluation of predictive models.

In this work, CO_2+O_2 hydrate dissociation points were measured at different O_2 mole fractions (11%, 32% and 50%) using isochoric pressure search method. In the second section of this paper, the experimental apparatus is described and the measured data are presented and checked. To predict the stability conditions of single-gas and mixed-gas hydrate systems, in the third section, a complete model for calculating hydrate-fluid and fluid-fluid phase equilibria is presented. It consists of a combination of the well-established hydrate theory of van der Waals and Platteeuw (vdWP) [15] with the e-PR-CPA Equation of State (EoS) [5].

2. Experimental

2.1. Materials

In Table 1, the suppliers of Carbon dioxide (CO_2, CAS Number: 124-38-9) and Oxygen (O_2, CAS Number: 7782-44-7) and the given purities are listed. Water (H_2O, CAS Number: 7732-18-5) was deionized and degassed.

Table 1: Chemical samples used for experimental work (CAS Registry Number, mole fraction purity and suppliers of chemicals).

Chemicals	CAS Reg. No.	Supplier	Purity (mol %)	Analysis method[a]
Carbon dioxide	124-38-9	Air Liquide	99.995	GC
Oxygen	7782-44-7	Air Liquide	99.999	GC
Water (ultrapure)	7732-18-5	MilliporeTM (direct-Q5)	18.2 MΩ·cm	

[a] GC: Gas Chromatography

Three mixtures of CO_2+O_2 were considered in this study, their compositions are listed in Table 2. The mixtures were prepared in a gas reservoir considering the difference of total pressure. First, the gas reservoir is put under vacuum. CO_2 was first introduced into the gas reservoir and the pressure was recorded (*P1*). Afterwards, O_2 is introduced and pressure is recorded (*P2*). The temperature of the gas reservoir is selected in order to have a monophasic phase inside. Approximate composition is estimated using $x_{O2}=(P2-P1)/P2$. In order to have the accurate value of the gas mixture composition, a Gas Chromatograph (Varian, model CP 3800), equipped with a thermal conductivity detector (TCD) is used. WINILAB III software (Perichrom, France) is used for peaks integration and their analysis. The calibration of the GC detector is obtained after introduction of several known pure component volumes. Appropriate syringes are considered. A PORAPAK R (80/100 mesh, 1.2 m X 1/8" Silcosteel) packed column is used. A calibration curve between moles number introduced and GC peak surface is determined and accuracies are determined. The resulting relative accuracies concerning the mole numbers are 0.7 % for CO_2 and 0.8 % for O_2. The uncertainty of molar fractions (x_1) is determined by Equation 1:

$$u(x_1) = x_1(1 - x_1)\sqrt{\left(\frac{u(n_1)}{n_1}\right)^2 + \left(\frac{u(n_2)}{n_2}\right)^2} \quad \textbf{(1)}$$

with $u(x_1)$ the uncertainty on mole fraction for component 1 and $\frac{u(n_i)}{n_i}$ the relative uncertainty on mole number n_i of the component i calculated from GC calibration.

Table 2: Compositions of the studied CO_2+O_2 mixtures: Expected composition and real composition mole fractions

Mixture	Expected composition mole fractions		Real composition mole fractions (x)		Standard uncertainties u(xCO_2)
	O_2	CO_2	O_2	CO_2	
MIX1	0.3	0.7	0.3238	0.6762	0.0016
MIX2	0.1	0.9	0.1104	0.8896	0.0006
MIX3	0.5	0.5	0.4984	0.5016	0.0015

2.2. Apparatus and method

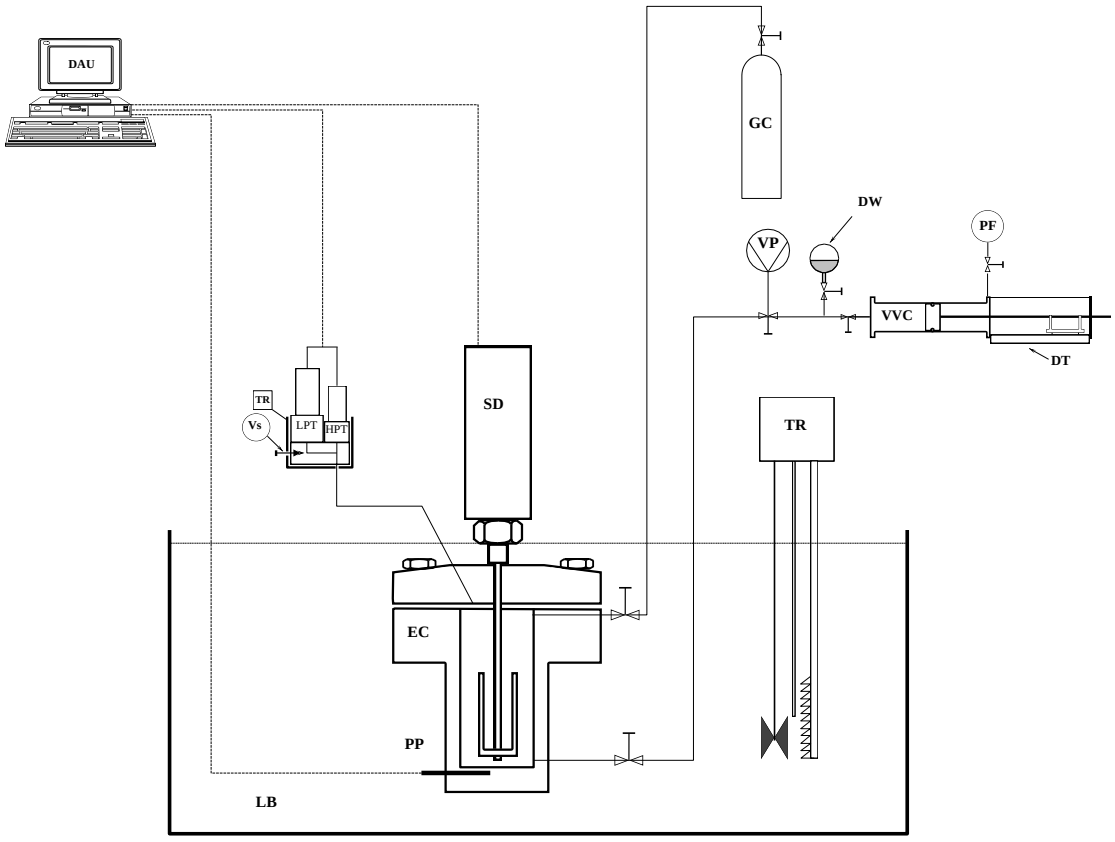

Figure 1: Schematic representation of the used apparatus. DW: degassed water; DAU: data acquisition unit; EC: equilibrium cell; GC: Gas cylinder; LPT: low pressure transducer; HPT: high pressure transducer; LB: liquid bath; PP: platinum probe; SD:

stirring de-vice; TR: temperature regulator; VP: vacuum pump; VVC: variable volume cell; PF: pressurizing fluid; DT: displacement transducer.

The principle of the experimental apparatus used to measure dissociation points of gas hydrates of the CO_2+O_2 mixture is based on the isochoric pressure search method. The experimental device is illustrated in Figure 1 and is the same one used in the previous work at Armines - Mines ParisTech [16-18]. It consists of a cylindrical constant volume (128 cm^3) equilibrium cell equipped with a Stirring Device (SD), two pressure transducers (LPT and HPT) to be more precise in each specific pressure range, a platinum resistance thermometer (PP) at the bottom of the cell (in aqueous phase) and introduced in a thermostatically controlled bath (LB) to maintain a constant temperature (TR). The evolution of temperature and pressure is monitored by means of a Data Acquisition Unit (DAU) connected to a DAU software to manage the stepwise variation of temperature and record the acquired data. The temperature probe (100 Ω) is calibrated against a 25-Ohm platinum resistance thermometer (model 5628, Fluke Hart Scientific) which is calibrated by LNE (Laboratoire National de Métrologie et d'Essais). The LPT and HPT pressure transducers were calibrated against pressure automated calibration equipment (PACE 5000, GE Sensing and Inspection Technologies) and a dead weight pressure balance (Desgranges & Huot 5202S, CP 0.3–40MPa, Aubervilliers, France), respectively.

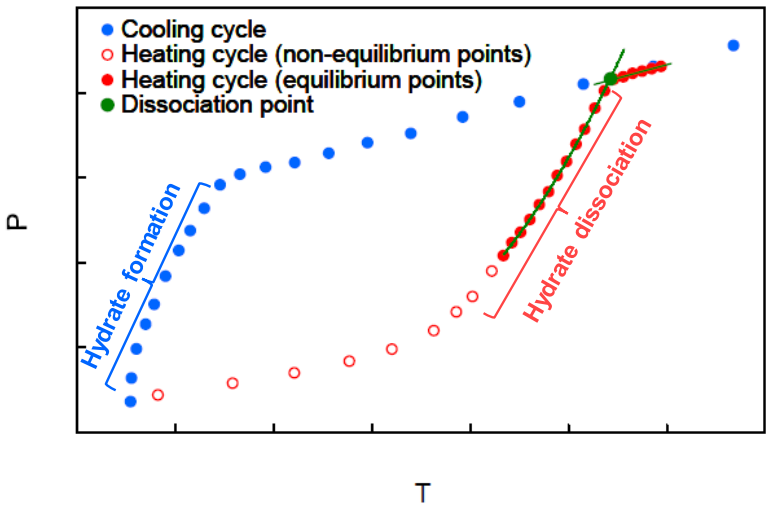

Figure 2: Measurement principle of gas hydrate dissociation points by isochoric pressure search method.

The measurement procedure summarized in Figure 2 consists of looking for the pressure at which the hydrates are completely dissociated. A gas mixture of a certain quantity and composition is introduced in the equilibrium cell which is previously evacuated and filled

with a known quantity of water. The mixture is then strongly agitated (800 RPM). The temperature is decreased until the hydrate phase is formed (sudden pressure drop). The temperature is then increased stepwise by 1K until the dissociation pressure of the hydrate phase is reached. For each step of temperature increase, equilibrium conditions are reached by allowing enough time at each step (8h/step). The hydrate dissociation point is determined by the intersection of the thermal expansion curve of the fluid and the equilibrium heating cycle curve. Once the hydrate dissociation point (P, T) is determined, more gas is added to the equilibrium cell to measure another point, and so on until enough experimental points are obtained. Finally, the equilibrium cell is emptied, cleaned and evacuated.

2.3. Experimental results

The expanded uncertainties $U = k \times u$ (with a coverage factor $k = 2$) are between 0.1 and 0.6 K for temperature ($U(T)$) and between 0.04 and 0.25 MPa for pressure ($U(P)$). The measured data are listed in Table 3 and presented in Figure 3a. The aqueous fraction (AqFr, see Equation 2), which is the ratio between the number of moles of water n_{H_2O} and the total number of moles in the system (water and gas $n_{H_2O} + \sum n_{gas}$), was determined for each measured point.

$$AqFr = x_{H_2O} = \frac{n_{H_2O}}{n_{H_2O} + \sum_{gas} n_{gas}} \quad \textbf{(2)}$$

Table 3: Measured data of hydrate dissociation conditions of the CO_2+O_2 gas mixture and expanded uncertainties (k=2): 0.10≤*U(T)*≤0.60 K and 0.040≤*U(p)*≤0.251 MPa.

Mixture	Loaded water		AqFr (mole fraction)	Temperature [K]	Pressure [MPa]
	n_{H_2O} (mole)	V_{H_2O} (cm^3)			
MIX1	1.16050	20.97	0.902 ± 0.017	274.17	2.178
	1.16050	20.97	0.886 ± 0.018	277.00	3.017
	1.16050	20.97	0.836 ± 0.015	279.75	4.233
	1.16050	20.97	0.761 ± 0.013	282.17	6.054
	1.16050	20.97	0.671 ± 0.010	283.88	8.353
	1.16050	20.97	0.550 ± 0.007	284.96	11.194
	2.04400	36.94	0.838 ± 0.009	283.26	7.227
	2.04400	36.94	0.681 ± 0.006	285.38	13.245
	2.80600	50.71	0.583 ± 0.006	286.07	18.741

MIX2	1.09190	19.73	0.965 ± 0.017	274.85	1.955
	1.09190	19.73	0.910 ± 0.015	277.84	2.810
	1.09190	19.73	0.843 ± 0.014	279.92	3.632
	1.09190	19.73	0.676 ± 0.010	282.37	5.590
	1.09190	19.73	0.523 ± 0.007	282.53	6.370
	1.09190	19.73	0.452 ± 0.005	282.69	6.799
MIX3	1.15004	20.78	0.912 ± 0.019	283.25	11.261
	1.15004	20.78	0.865 ± 0.018	284.32	13.895
	1.15004	20.78	0.848 ± 0.018	285.01	15.985
	1.15004	20.78	0.956 ± 0.021	275.79	4.460
	1.15004	20.78	0.945 ± 0.020	278.98	6.299
	1.15004	20.78	0.916 ± 0.020	282.39	9.713

A consistency test was applied to the measured data. Using the Clausius-Clapeyron relation (Equation 3) [19], the evolution of the enthalpy of dissociation of the hydrate as a function of temperature is examined. Given the small temperature range, we can consider that the compressibility factor does not vary significantly, and since the enthalpy of dissociation does not vary rapidly [19], this equation can be used in a small dissociation temperature range to check the linearity of the measured data in terms of $ln(p)$ as a function of $1/T$.

$$\frac{dln(P)}{d\left(\frac{1}{T}\right)} = \frac{-\Delta H_{dis}}{Z\ R} \quad \textbf{(3)}$$

where P and T are respectively the hydrate dissociation pressure and temperature (in equilibrium with the vapor (or liquid) and aqueous phases), R the ideal gas constant, Z the compressibility factor and ΔH_{dis} the apparent enthalpy of dissociation of the hydrate phase.

The results of the consistency tests on the measured data are shown in Figure 3 (b, c and d). Overall the measured data are consistent. . When a breakpoint is present, it means that we have gas hydrate when there is a phase split in the gas-rich phase (CO_2+O_2) including a vapor phase and a CO_2-rich liquid phase (other than the aqueous phase). In the modeling part (next section), the phase behavior (single-phase and two-phase) of the gas mixture in equilibrium with the aqueous phase and the hydrate phase is highlighted for the different CO_2+O_2 mixture compositions.

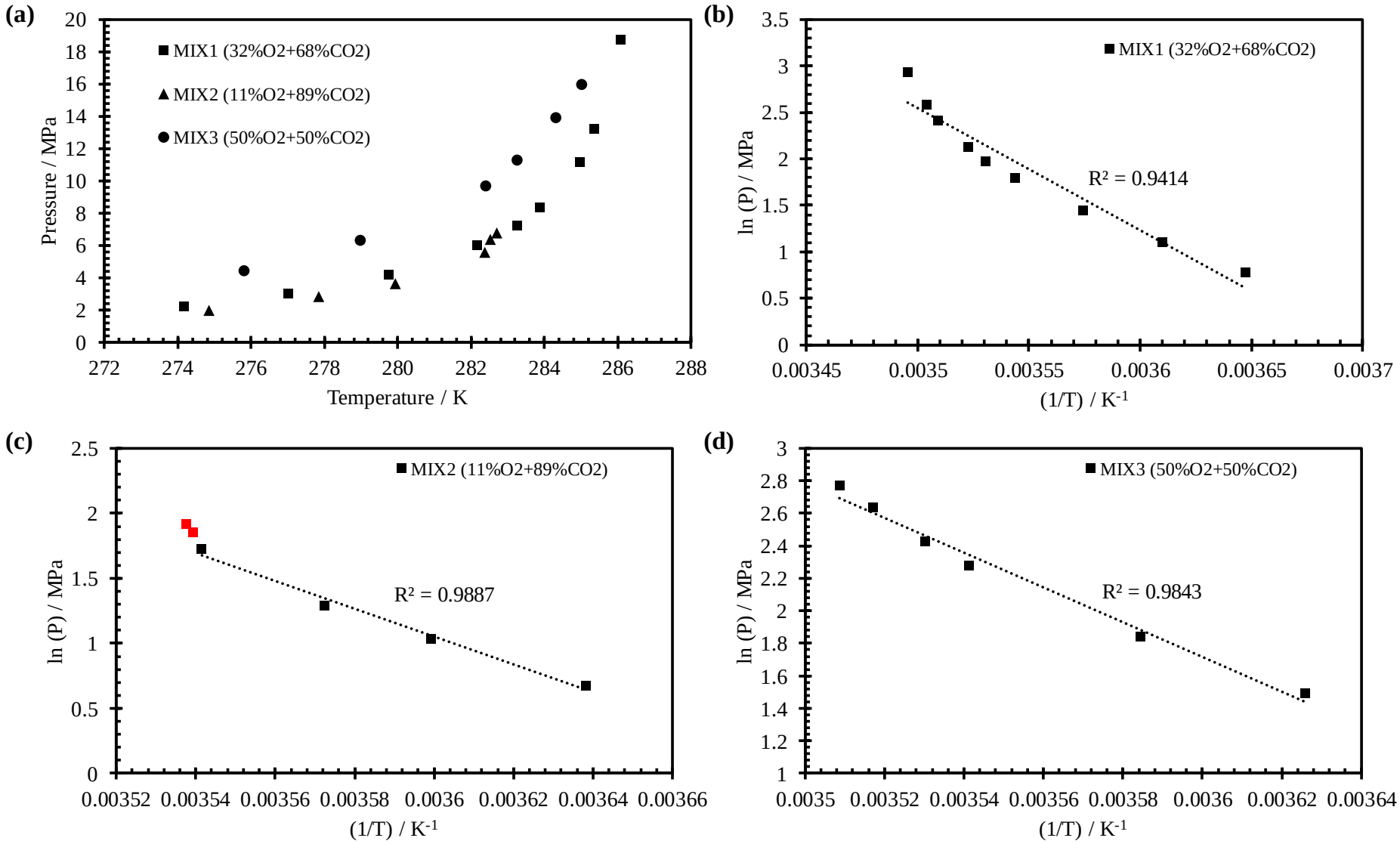

Figure 3: Hydrate dissociation points of the CO_2+O_2 gas mixture: measured data (a) and consistency tests (b, c and d). The red symbols (graph c) represent measurements where the gas mixture was in liquid-vapor equilibrium (see Figure 9b).

3. Thermodynamic modeling

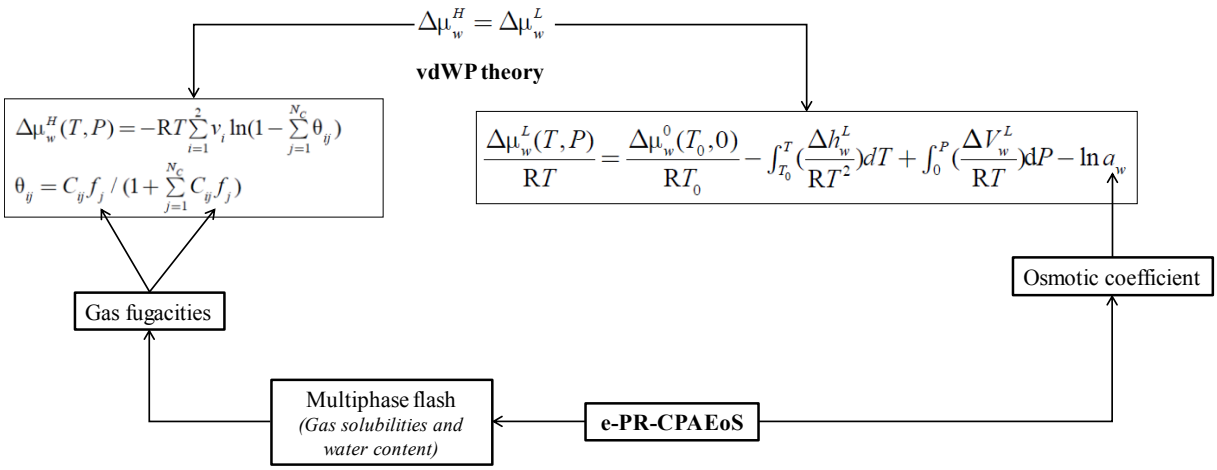

Figure 4: Schematic diagram of the approach used to calculate gas hydrate equilibria with the e-PR-CPA model combined with the Van der Waals and Platteeuw model.

3.1. Model presentation: procedure description and parameter estimation

Hydrate dissociation thermodynamic modeling is generally done by combining the solid van der Waals and Platteeuw theory [15] for hydrate phase calculation with an Equation of State (EoS) for fluid phases (liquid and vapor) calculation and possibly with a G-excess model for water activity coefficient estimation. The hydrate dissociation curve represents the equilibrium of the hydrate phase with the aqueous phase and the gas-rich phase (which can be liquid and/or vapor), and this more or less limits the hydrate stability domain at thermodynamic equilibrium. The e-PR-CPA (electrolyte Peng-Robinson Cubic Plus Association) EoS recently developed and presented in our previous work [5-7] has performed successfully in the prediction of liquid (gas solubility) and vapor (water content) phases of systems including water, gas (CO_2, O_2, H_2, CH_4, etc.) and salt (NaCl). Hence, this EoS has been chosen to calculate gas fugacities, fluid phase (aqueous and gaseous) equilibria, and the activity coefficient of water which is different from one if there are electrolytes (salts) or solvents (alcohols, glycols, etc.) in the aqueous solution.

For the calculation of fluid phase equilibria with an equation of state, it is necessary to know the overall composition (or feed composition) of the system. However, generally, mixed-gas hydrate data are provided in terms of "water-free" gas composition x'_{gas} ($\sum_{gas} x'_{gas} = 1$) and aqueous fraction AqFr ($= x_{H_2O}$) (see Equation 2) in order to study hydrates with a fixed global gas mixture composition. In order to be able to model mixed-gas hydrate systems, we

provide below the equations used to convert these "apparent" quantity (x'_{gas}) into "real" mole fractions x_i ($\sum_i x_i = 1$, $i =$ all non-electrolyte species).

Using Equation 2, the mole number of water is:

$$n_{H_2O} = \frac{AqFr \sum_{gas} n_{gas}}{1 - AqFr} \quad \textbf{(4)}$$

Considering a total mole number of 1 for the gas mixture ($\sum_{gas} n_{gas} = 1$ and $n_{gas} = x'_{gas}$), the Equation 4 becomes:

$$n_{H_2O} = \frac{AqFr}{1 - AqFr} \quad \textbf{(5)}$$

Finally, the real mole fractions are calculated by:

$$x_i = \frac{n_i}{n_{H_2O} + \sum_{gas} n_{gas}} = \frac{n_i}{n_{H_2O} + 1} = \frac{n_i}{\frac{AqFr}{1 - AqFr} + 1} \quad \textbf{(6)}$$

Applying Equation 6 to water and a gas *i*, we obtain:

$$x_{H_2O} = \frac{n_{H_2O}}{\frac{AqFr}{1 - AqFr} + 1} = \frac{\frac{AqFr}{1 - AqFr}}{\frac{AqFr}{1 - AqFr} + 1} = AqFr \quad \textbf{(7)}$$

$$x_{gas,i} = \frac{n_{gas,i}}{\frac{AqFr}{1 - AqFr} + 1} = \frac{x'_{gas,i}}{\frac{AqFr}{1 - AqFr} + 1} \quad \textbf{(8)}$$

The aqueous fraction has no effect on single-gas hydrate systems, since in two-phase thermodynamic equilibrium (which is always the case for gas-water systems), the calculation of the compositions in each phase of a binary system is independent of the global composition (using Gibbs' phase rules, the degree of freedom is two in this case, for example, in a liquid-vapor PT-flash calculation, the same results of liquid x and vapor y compositions are obtained for any global composition z stable in the liquid-vapor state). However, for mixed-gas hydrate systems, the degree of freedom is higher than two, hence calculations of the hydrate dissociation conditions are sensitive to the aqueous fraction, and the composition of the gas-

rich phase can vary significantly from the overall composition if one of the gases is more absorbed than the other in the hydrate.

At thermodynamic equilibrium, one can write the equality of the chemical potential of water in the liquid phase and in the hydrate phase. As illustrated in the schematic of Figure 4, the e-PR-CPA model calculates gas fugacities and the osmotic coefficient of water which is then transformed into water activity (Equation 10), in order to calculate the chemical potential of water in the liquid and hydrate phases. A multiphase flash [20, 21] is calculated at each step until the Hydrate-Liquid-Vapor (HLV) or Hydrate-Liquid-Liquid (HLL) equilibrium is reached. Newton's method was applied to find the dissociation pressure at fixed temperature and the dissociation temperature at fixed pressure. The different terms of the vdWP model (Figure 4) were calculated by the Munck et al. [22] method.

The vdWP model derived from statistical thermodynamics is an established theory for the study of phase equilibria involving hydrates following the implementation proposed by Parrish and Prausnitz [23]. Since then, several studies have been published using this approach, therefore the vdWP model is very well described in the literature. The equations proposed by Munck et al. [22] have been used in this work for the calculation of the chemical potential of water in the liquid and hydrate phase. However, since we use a different equation of state, a reparameterization of the parameters used in the calculation of the Langmuir constant is necessary.

A. e-PR-CPA EoS

A detailed description of the e-PR-CPA EoS equations and parameterization is given in our previous work [5]. However, we recall here the main terms and definitions of the parameters. For the modeling of complex systems including gas, water and ions, the e-PR-CPA EoS (expressed in terms of reduced residual Helmholtz free energy $\frac{A^{res}_{e-PR-CPA}}{RT}$ in Equation 9) combines several terms to represent the different types of interactions in these systems. For molecular interactions, the selection concerns the well-known cubic term of Peng-Robinson (PR) [24] to describe attractive and repulsive forces between species, and the Wertheim's association theory [25] used in SAFT and CPA –type EoS to describe association phenomena (self-association between identical molecules and cross-association between different molecules). For electrolyte interactions, the MSA theory (Mean Spherical Approximation) [26]

and the Born term [27] were chosen to represent ion/ion and ion/solvent (solvation) interactions, respectively.

$$\frac{A^{res}_{e-PR-CPA}}{RT} = \frac{A^{PR}}{RT} + \frac{A^{Association}}{RT} + \frac{A^{MSA}}{RT} + \frac{A^{Born}}{RT} \quad \textbf{(9)}$$

Like most thermodynamic models, the parameterization of the e-PR-CPA EoS on pure and binary systems will allow to predict multicomponent (ternary, quaternary, etc.) systems. However, comparison with some experimental data is necessary to verify if the model is well adapted to the studied systems. Concerning fluid phase equilibria modeling, the e-PR-CPA EoS counts for pure compounds:

- Five parameters for the solvent (water): three parameters (m_i, $a_{0,i}$, b_i) to determine the energy parameter a_i and the co-volume b_i in the PR cubic term, and two parameters (association energy ε_i and bonding volume β_i) to calculate the Wertheim association term.
- Three parameters for each ion: three parameters (m_{ion}, $a_{0,ion}$ and ion diameter σ_{ion}) for the calculation of the energy parameter a_{ion} and the co-volume b_{ion} in the PR cubic term.
- No parameters for the gas (only the critical temperature T_c and pressure P_c and the acentric factor ω must be known, which is the case for all gases).

Halite is the main and almost "the only pure" mineral in salt layers where storage caverns are built, hence the water+NaCl mixture was chosen as a representative brine mixture. Before modeling phase equilibria involving fluid and hydrate phases, the osmotic coefficient ∅ of the aqueous electrolyte water+NaCl and the two-phase equilibria calculated by the e-PR-CPA must be verified. In Figure 5, the calculations at different salinities (in terms of NaCl molality: m=[mol/kg_w]) of the vapor pressure and the osmotic coefficient of the water+NaCl system by the e-PR-CPA EoS were compared with experimental literature data. As shown in the figure, the model accurately correlates these two properties and estimates their variation as a function of temperature and NaCl molality. The water activity a_w used to calculate the chemical potential of water in the liquid phase (see Figure 4) is easily obtained from the osmotic coefficient ∅ by the following relationship (Equation 10):

$$a_w = \exp\left[-\frac{M_{H_2O}}{1000}\left(\sum_{ion} m_{ion}\right)\emptyset\right] \quad \textbf{(10)}$$

where M_{H_2O} is the molar mass of water and m_{ion} is the molality of each ion (Na+ and Cl- in our case).

Concerning binary systems, generally a Binary Interaction Parameter (BIP or k_{ij} in the cubic term) is to be determined in particular for binaries whose species are not associative. However, for mixtures of associative compounds, when solvation is possible, the cross-association volume β_{ij} can be considered as a second adjustable parameter in order to improve the calculations [28]. Since the e-PR-CPA EoS is reduced to the PR EoS in the case of systems that do not contain associative compounds and electrolytes (e.g. gas mixtures), it is possible to use parameters already available in the literature to represent this type of system. In Table 4, the different parameters of the e-PR-CPA model as well as the thermophysical properties used for their determination (by optimization) are presented.

The parameters of the pure compounds as well as the interaction parameters of the CO_2+H_2O+NaCl and O_2+H_2O+NaCl systems used in this work are from our previous work [5, 6]. The binary interaction parameter ($k_{CO_2-O_2} = 0.114$) used to represent Vapor Liquid Equilibria (VLE) of the CO_2-O_2 binary system was taken from the work of Lasala et al. [29].

In Figures 6 and 7, the predictions of the VLE of the CO_2+H_2O+NaCl, O_2+H_2O+NaCl and CO_2+O_2 systems by the e-PR-CPA EoS are compared to the experimental data. As shown in the figures, the e-PR-CPA EoS accurately estimates gas solubility in water and brine (Figures 6a and 6b) and water content in gas-rich phases (Figure 7a) and captures very well the salting-out effect of gas due to the presence of NaCl under different thermodynamic conditions. The complete study of these systems as well as precise solubility data tables are provided in our previous work [6]. The VLE of the CO_2+O_2 gas mixture calculated by the same model which is reduced to the PR EoS (since there are no electrolytes or associative compounds) are quite good, however this representation can be improved especially in the region of the critical points of the mixture by using other mixing rules (see Lasala et al. [29] and Ahamada et al. [4]), multiparametric EoS (e.g. EoS-CG), or adding a crossover treatment (see Dicko and Coquelet [30] and Janecek et al. [31]). All these options add additional parameters, which is not necessary for our study, as demonstrated by the prediction results obtained for multicomponent systems (see section 3.3).

The water activity and fluid phase equilibria are known, to model gas hydrate systems following the approach described earlier, it remains to determine the Langmuir constants C_{ij}

of each gas j in a cavity of type i (two types of cavities exist for hydrates: small and large cavities).

B. Langmuir constant

The Langmuir constants quantify the interactions between guest (gas) and host (water) molecules in hydrate cavities. Generally, the formula (Equation 11) proposed by van der Waals and Platteeuw [15] developed using the Lennard-Jones-Devonshire cell theory (considering a spherically symmetrical cell) is used to determine the Langmuir constants. For this, the Kihara potential [32] (McKoy and Sinanoğlu [33]) whose parameters are adjusted on experimental hydrate stability data is used to calculate the spherically symmetrical cell potential $W(r)$.

$$C_{ij}(T) = \frac{4\pi}{kT}\int_0^{\infty} \exp\left[-W(r)/kT\right] r^2 dr \qquad \textbf{(11)}$$

where k is Boltzmann's constant, T is the temperature and r is the cell radius.

In order to avoid the numerical calculation of the integral in Equation 11, Parrish and Prausnitz [23] proposed a simplified empirical expression (Equation 12) of the Langmuir constant which was then used and refined in subsequent studies (e.g. the notable work by Munck et al. [22]).

$$C_{ij}(T) = \frac{A_{ij}}{T}\exp\left(\frac{B_{ij}}{T}\right) \qquad \textbf{(12)}$$

In Equation 12, the A_{ij} and B_{ij} coefficients are specific to gas and cavity types (small or large) and are optimized on experimental gas hydrate data. In this work we have used similar empirical relationships inferred from the shape of the Langmuir constants (for each gas and cavity type) variation with respect to temperature. The coefficients of these formulations are determined by minimizing the absolute deviation between the calculated gas hydrate dissociation pressure or temperature data and the experimental data. The expressions of the Langmuir constants obtained for CO_2 and O_2 in Small and Large cavities are as follows:

$$C_{Small,CO_2} = 74832.46337816 \exp\left(-0.08827493\ T\right) \quad \textbf{(13)}$$

$$C_{Large,CO_2} = \frac{4.19 \times 10^{-7}}{T} \exp\left(\frac{2813}{T}\right) \quad \textbf{(14)}$$

$$C_{Small,O_2} = 0.04462485 \exp\left(-0.04019974\ T\right) \quad \textbf{(15)}$$

$$C_{Large,O_2} = 0.00132256 \exp\left(-0.02147978\ T\right) \quad \textbf{(16)}$$

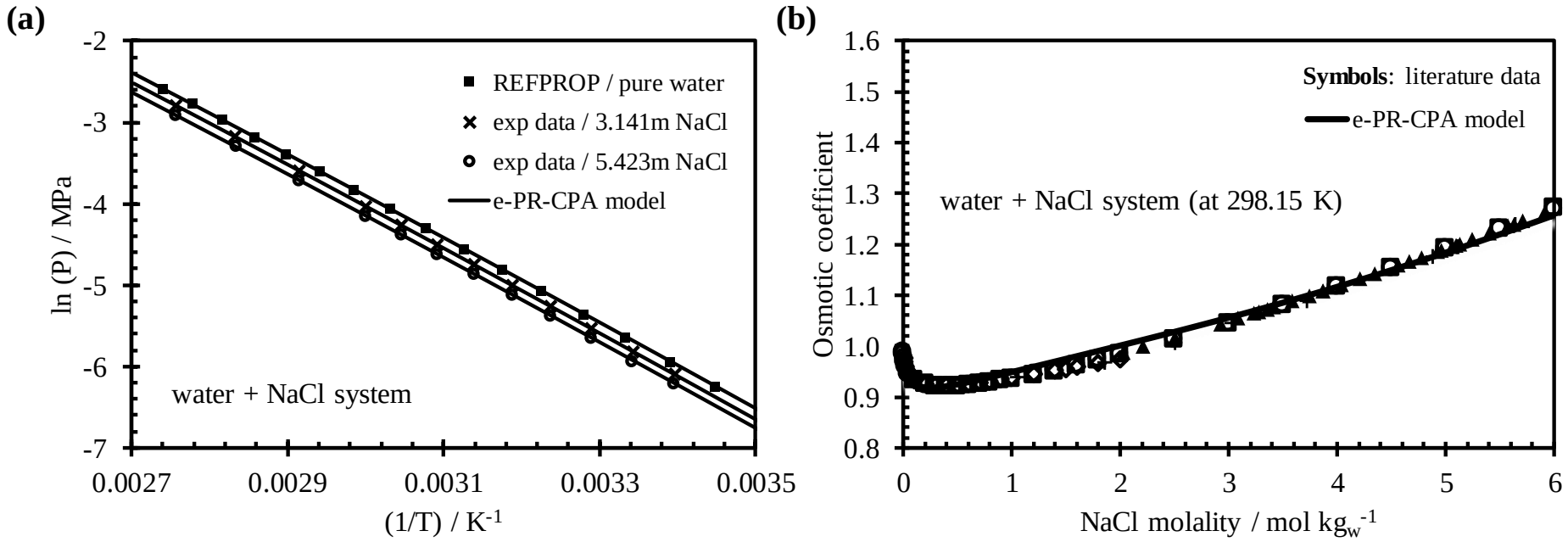

Figure 5: Saturation vapor pressure (a) and osmotic coefficient (b) of H_2O + NaCl system. Comparison of literature data (symbols) [34-40] with predictions (solid lines) by e-PR-CPA EoS.

Table 4: e-PR-CPA EoS configuration: model parameters and properties used in the fitting.

		$\frac{A^{PR}}{RT}$	$\frac{A^{Association}}{RT}$	$\frac{A^{MSA}}{RT}+\frac{A^{Born}}{RT}$	Adjusted on:
Pure	gas	-	-	-	-
	ions	m_i, $a_{0,i}$	-	σ_{ion}	Vapor pressure and osmotic coefficient
	water	a_0, m, b	ε, β	-	Vapor pressure and density
Binary	gas-gas	$k_{gas-gas}$	-	-	Vapor Liquid Equilibria (VLE) data
	gas-water	$k_{gas-water}$	$\beta_{gas-water}$ (if solvation, e.g CO_2)	-	Gas solubility in water
	gas-ions	$k_{gas-anion}$ $k_{gas-cation}$	-	-	Gas solubility in water + salt

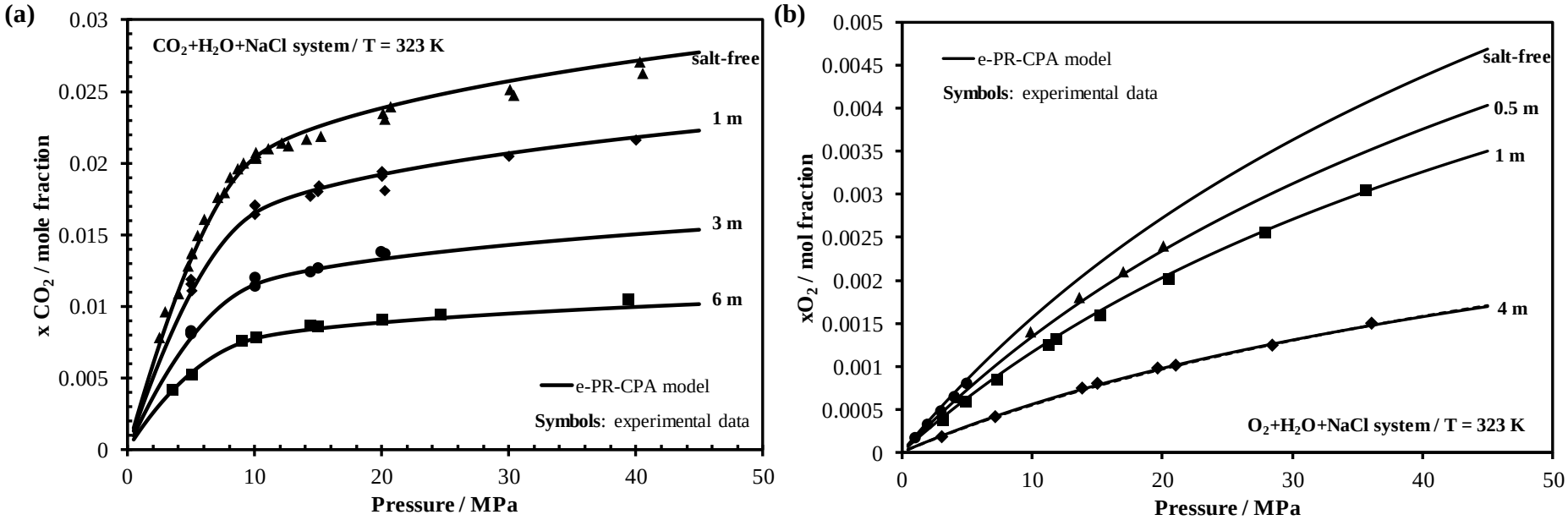

Figure 6: Comparison of experimental data (symbols) [6, 41-49] with predicted CO_2 (a) and O_2 (b) solubilities in NaCl-brine at 323 K for different salt molalities using the e-PR-CPA EoS (solid lines).

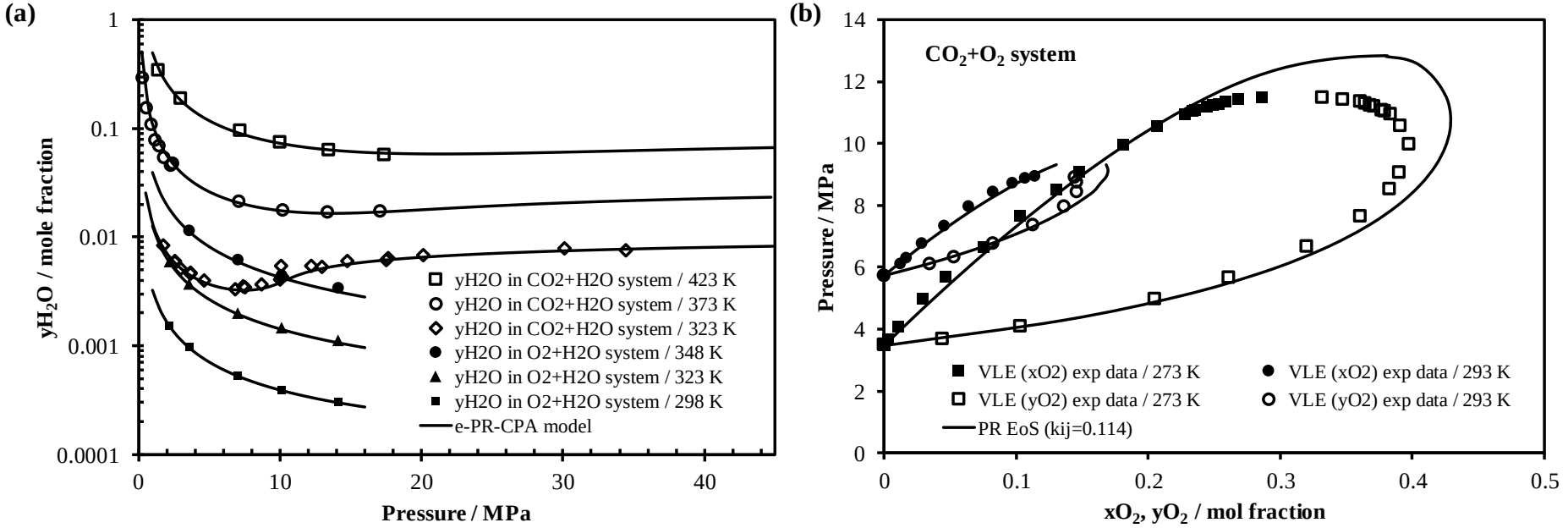

Figure 7: Water content in CO_2+H_2O and O_2+H_2O systems (a) and VLE of the CO_2+O_2 mixture (b) at different temperatures: Comparison of experimental data (symbols, (a): [47, 48, 50-54]; (b): [29]) with predictions (solid lines) using e-PR-CPA model (a) and PR EoS (b).

3.2. Hydrate stability of the O_2+H_2O and CO_2+H_2O+(NaCl) mixtures

Structures I and II are the most common forms of gas hydrates [55]. From a modeling point of view, the most stable hydrate structure is the one with the lowest dissociation pressure. Pure CO_2 is well known to form hydrate of structure I. The (e-PR-CPA + vdWP) model predicts a type I hydrate structure for CO_2 hydrate and this is also the case for O_2. The latter is a subject of discussion, basically it has been considered in the past that O_2 forms type I hydrate (like any other small molecule) but later experimental studies [56, 57] have shown that it rather forms type II hydrates. However, according to different studies carried out at different temperature ranges, it is found that O_2 at low temperatures (<270 K) forms type II hydrates and forms type I hydrates at higher temperatures [58] which is the case in our study.

The modeling results of the stability conditions of O_2 hydrate in pure water and CO_2 hydrate in pure water and NaCl-brine are shown in Figure 8. By comparing with experimental literature data, the developed model (e-PR-CPA + vdWP) correlates accurately the gas hydrate data in pure water and also predicts well the inhibitory effect of NaCl on the stability of CO_2 hydrate at different concentrations (in terms of salt molality) which tends to destabilize the hydrate proportionally to its concentration. Model calculations are reliable over a wide range of temperature and pressure (up to 100 MPa) for gas hydrates in pure water. The high quality predictions of the effect of salt (NaCl) on CO_2 hydrates is due to the accurate representation of the salting-out effect by the e-PRCPA EoS and also to the excellent vdWP hydrate theory. In addition, it should be noted that the model has been successfully applied to other single-gas and mixed-gas hydrate systems (CH_4+H_2O, CH_4+H_2O+NaCl and CH_4+CO_2+H_2O etc.).

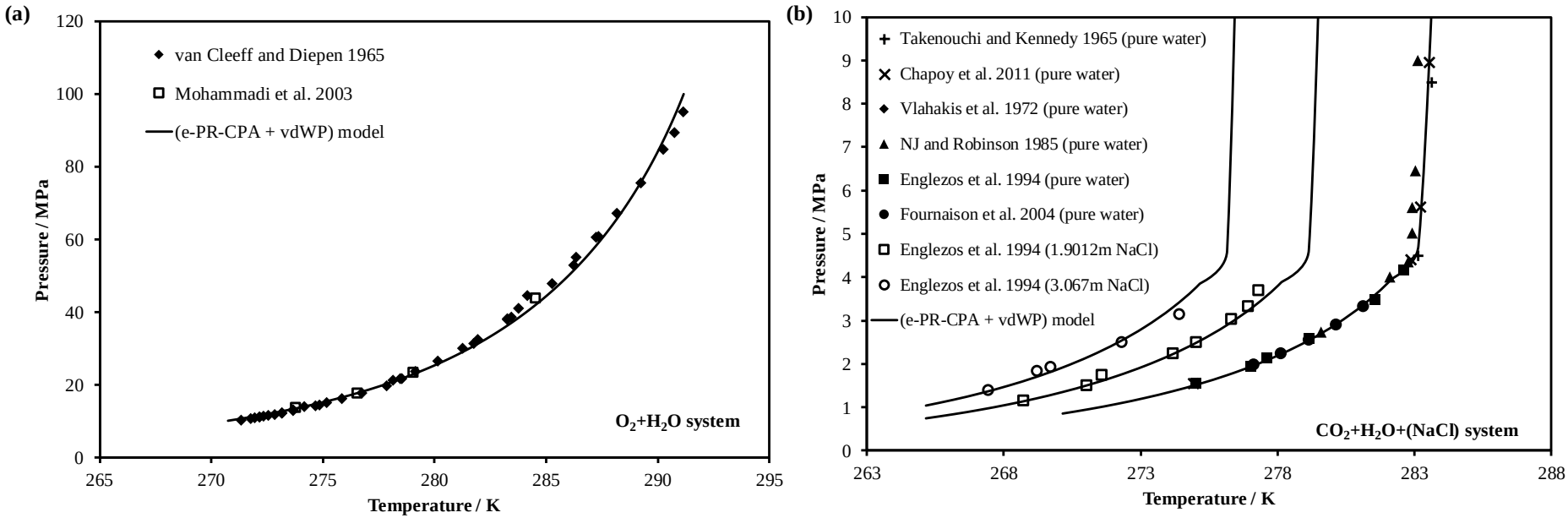

Figure 8: Hydrate dissociation conditions of the O_2+H_2O (a) and CO_2+H_2O+(NaCl) (b) mixtures: Comparison of literature experimental data with predictions using the (e-PR-CPA + vdWP) model.

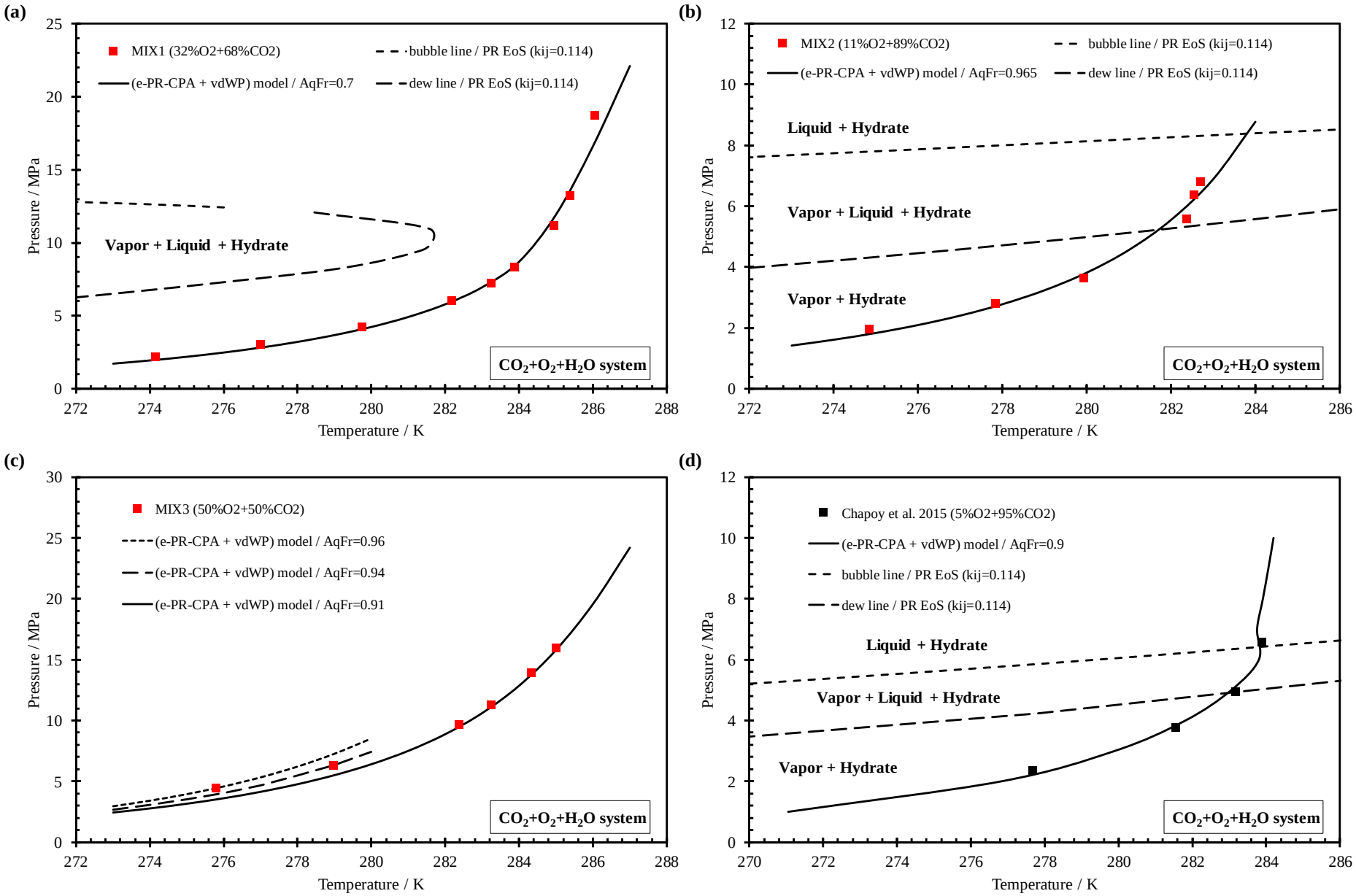

Figure 9: Hydrate dissociation conditions of the CO_2+O_2+H_2O ternary system at different O_2 "water-free" mole fractions 32% (a), 11% (b), 50% (c) and 5% (d): Comparison of measured (a, b and c, see Table 3) and literature [11] (d) experimental data with predictions using the (e-PR-CPA + vdWP) model (solid lines). The bubble and dew lines of the different gas mixtures are determined by the PR EoS.

3.3. Hydrate stability of the CO_2+O_2+H_2O mixture

Concerning the mixed-gas hydrate system (CO_2+O_2), the (e-PR-CPA + vdWP) model also predicts a hydrate structure of type I. In Figure 9, the predictions of the hydrate stability conditions of this system are compared with the measured data (from this work, see Table 3) at different O_2 compositions (11%, 32% and 50% water-free mole fraction) and also with those of Chapoy et al. [11] at 5% O_2. Remarkable accuracy in the predictions of this system at different gas mixture compositions from 5 to 50% O_2 is obtained. The calculations were performed at different fixed aqueous fractions AqFr in a very representative way of the experimental aqueous fractions listed in Table 3 which are not fixed (decreases with each increase in pressure by adding more gas mixture). It should be noted that no further adjustments were made, i.e. only the good representation of the single-gas hydrate systems and the VLE of the binary systems (gas-gas and gas-water) allowed the accurate prediction of the multi-component system (CO_2+O_2+H_2O), and this is thanks to the good theoretical basis of the coupling of the e-PR-CPA EoS with the vdWP theory. As shown in Figure 9, by plotting the gas hydrate dissociation curve and the phase envelope of the gas mixture obtained by the e-PR-CPA model, we can accurately identify the different types of coexisting phases (liquid, aqueous, vapor and gaseous) at each temperature and pressure condition, which is very useful. As shown in plots a, b, c and d of Figure 9, the addition of O_2 effectively decreases the critical point of the mixed-gas and shifts its phase envelope to lower temperatures, and it seems that the 50% O_2 mixture or even less the 32% O_2 mixture are preferred to ensure that there is no phase change (especially phase split to liquid-vapor equilibrium) in the gas stored in the cavern.

For an overview, in Figure 10, the hydrate stability results of the ternary CO_2+O_2+H_2O system are plotted from pure CO_2 hydrate to pure O_2 hydrate, showing the effect of oxygen on the stability of the CO_2-rich mixed-gas hydrate. This Figure shows that at high pressure (>20 MPa) the hydrate dissociation temperature of the mixed gas CO_2+O_2 becomes higher than that of pure CO_2, therefore precautions must be taken to avoid hydrate formation at the wellhead or in the pipelines during the transport of this gas stream which is assumed to be saturated with water vapor after its withdrawal from the cavity. However, in reality the stored gas is in equilibrium with almost “pure” NaCl-brine and not pure water, which led us to study in the following section the effect of NaCl on this mixed-gas system.

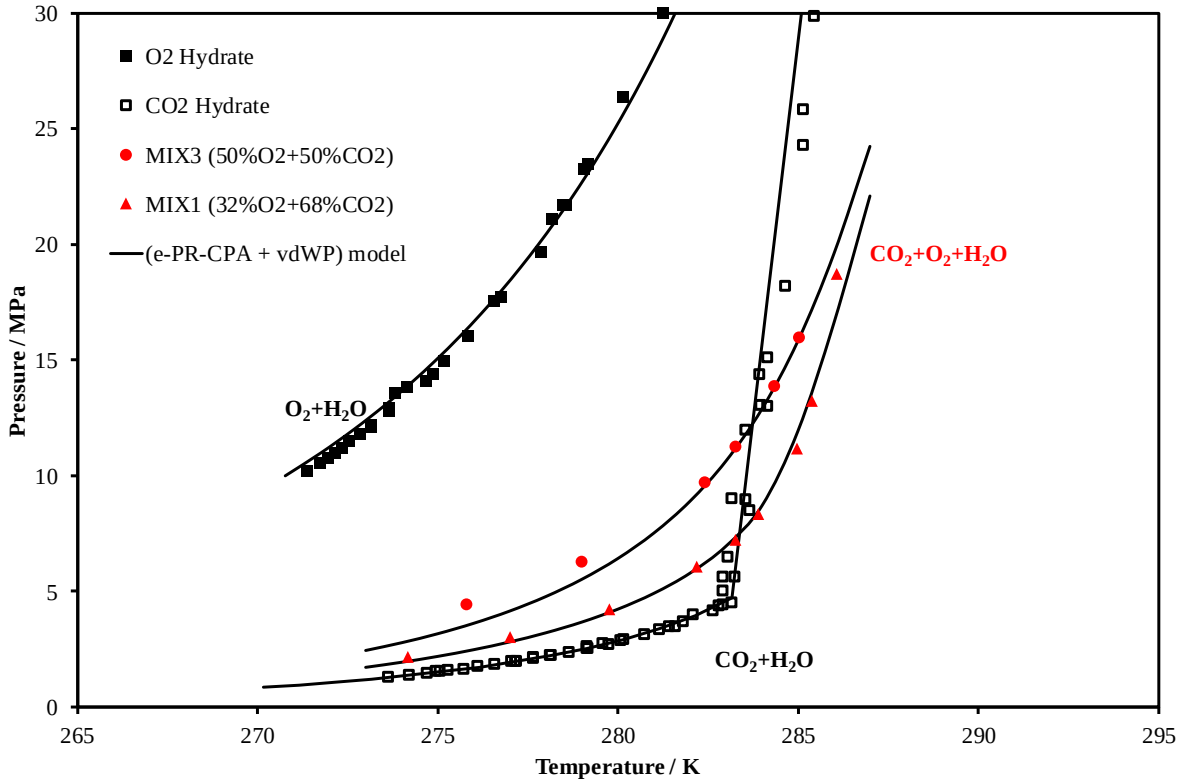

Figure 10: Hydrate dissociation conditions of the CO_2+O_2+H_2O ternary system from pure O_2 hydrate to pure CO_2 hydrate. Comparison of literature and measured data with predictions using the (e-PR-CPA + vdWP) model (solid lines).

3.4. Hydrate stability of the CO_2+O_2+H_2O+NaCl mixture

The developed model (e-PR-CPA + vdWP) has shown its predictive capabilities, in particular the transition from simple binary systems to multi-component systems (gas+water+salt and mixed-gas+water). Since all the necessary parameters are already available, in particular the interaction parameters CO_2+O_2, O_2-Na+, O_2-Cl-, O_2-H_2O, CO_2-Na+, CO_2-Cl- and CO_2-H_2O, we can model the quaternary system CO_2+O_2+H_2O+NaCl with a high degree of confidence. The study of this system involves several variables including the composition of the mixed-gas, the aqueous fraction and the salinity (NaCl molality). Taking the example of the FluidSTORY project on the combination of the Power-to-Gas (PtG) and Underground Gas Storage (UGS) technologies discussed earlier in the introduction, the quantity of O_2 in the EMO unit is relatively less than CO_2 [59], that is why we choose to study the mixture with 32% O_2. The aqueous fraction was kept the same (AqFr=0.7) as that of the mixed-gas system (without salt, see Figure 9a) with 32% O_2, as well as two salinities were studied (1m and 4m), one was limited to 4m since the O_2 solubility data in NaCl brine on which the e-PR-CPA EoS was adjusted are limited to this salinity (4m, see Chabab et al. [6]).

The modeling results obtained are shown in Figure 11. As expected, NaCl significantly decreases the hydrate dissociation temperature of this gas mixture. The shape of the curve remains the same with a shift to the left by adding the salt. The model also detects when there are several phases in equilibrium especially at 4m when the hydrate dissociation curve crosses the phase envelope of the gas mixture. According to the trend of the dissociation points calculated by the model in this region, we notice from the slight change in the curve that there is a phase split and that at a pressure higher than the bubble line and at the left of the gas hydrate dissociation curve, the hydrate is rather in equilibrium with a gas-rich liquid phase and not with a vapor phase.

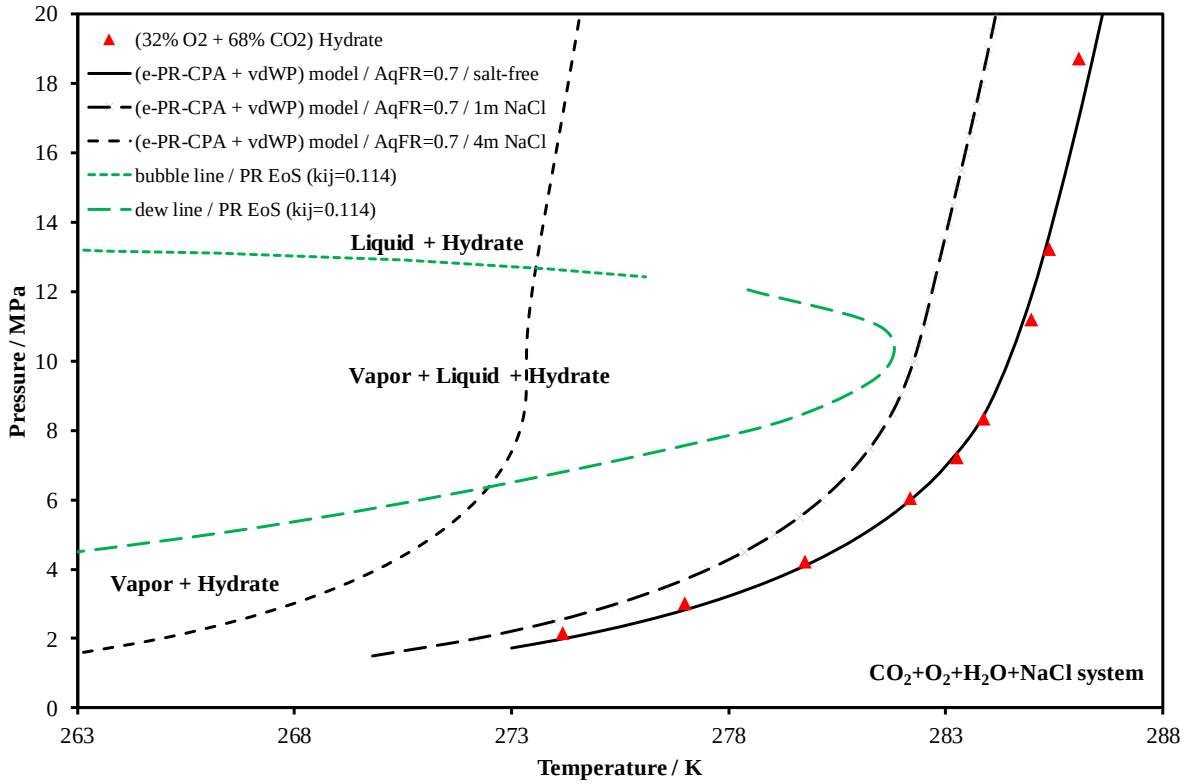

Figure 11: Hydrate dissociation conditions of the CO_2+O_2+H_2O+(NaCl) quaternary system: Prediction of the effect of NaCl concentration (from salt-free to 4m) on the mixed-gas hydrate system (32% O_2 , at fixed aqueous fraction AqFr=0.7) using the (e-PR-CPA + vdWP) model. The bubble and dew lines are determined by the PR EoS.

4. Conclusions

In this work the phase behavior of systems containing CO_2, O_2, H_2O and possibly NaCl, and in particular the gas hydrate stability conditions of CO_2, O_2 and their mixtures were studied. The isochoric pressure search method was used to overcome the lack of data for the CO_2+O_2+H_2O system by measuring new hydrate dissociation points of the CO_2+O_2 gas mixture at different global compositions. The consistency of the measured data was verified using the Clausius-Clapeyron relationship. In addition to the fact that these data were measured for a promising massive energy storage application (combination of PtG with UGS using the EMO process), these data will serve for the evaluation of predictive models, and also to help to avoid problems related to flow assurance by taking the necessary precautions when transporting gas streams composed of CO_2, O_2 and water, for instance, oxycombustion flue gas.

To predict the dissociation conditions of gas hydrates, in this work, the established hydrate theory of van der Waals and Platteeuw (vdWP) is combined with the e-PR-CPA EoS which has shown in this and previous work excellent capabilities to determine water activity in brine, gas solubility in water and brine and to predict the water content in gas-rich phase. The resulting model (e-PR-CPA + vdWP) was successfully applied to the O_2+H_2O and CO_2+H_2O+NaCl systems by comparing with literature data as well as to the CO_2+O_2+H_2O mixed-gas hydrate system by comparing predictions with the new reported measurements. The model allowed a complete study of phase equilibria (hydrate-fluids and fluid-fluids) of gas/water systems and also to accurately predict the effect of the presence of salt on the stability of gas hydrates. The excellent results obtained using this model for single-gas and mixed-gas hydrate systems without adding additional parameters for the latter are the result of an advanced equation of state (e-PR-CPA) and a theoretically solid solution for gas hydrates (vdWP).

Supporting Information (SI)

Tables of CO_2 and O_2 hydrate dissociation data in water and NaCl brine in a wide range of pressure and temperature.

Acknowledgments

We thank Dr. Martha Hajiw for the various useful discussions. Financial support from Agence Nationale de la Recherche (ANR) through the project FluidSTORY (n° 7747, ID ANR-15-CE06-0015) is gratefully acknowledged.

References

1. Habibi, R., An investigation into design concepts, design methods and stability criteria of salt caverns. *Oil Gas Sci. Technol.* **2019,** 74, 14.
2. Merey, S., Prediction of pressure and temperature changes in the salt caverns of Tuz Golu underground natural gas storage site while withdrawing or injecting natural gas by numerical simulations. *Arabian J. Geosci.* **2019,** 12, 205.
3. Kleinitz, W.; Boehling, E. In *Underground gas storage in porous media–operating experience with bacteria on gas quality (spe94248)*, 67th EAGE Conference & Exhibition, 2005; European Association of Geoscientists & Engineers: 2005; pp cp-1-00556.
4. Ahamada, S.; Valtz, A.; Chabab, S.; Blanco-Martin, L.; Coquelet, C., Experimental density data of three carbon dioxide and oxygen binary mixtures at temperatures from 276 to 416 K and at pressures up to 20 MPa. *J. Chem. Eng. Data* **2020,** Submitted.
5. Chabab, S.; Théveneau, P.; Corvisier, J.; Coquelet, C.; Paricaud, P.; Houriez, C.; El Ahmar, E., Thermodynamic study of the CO2–H2O–NaCl system: Measurements of CO2 solubility and modeling of phase equilibria using Soreide and Whitson, electrolyte CPA and SIT models. *Int. J. Greenhouse Gas Control* **2019,** 91, 102825.
6. Chabab, S.; Ahmadi, P.; Théveneau, P.; Coquelet, C.; Chapoy, A.; Corvisier, J.; Paricaud, P., Measurements and modeling of high-pressure O2 and CO2 solubility in brine (H2O+NaCl). *J. Chem. Eng. Data* **2020,** Accepted (In press).
7. Chabab, S.; Théveneau, P.; Coquelet, C.; Corvisier, J.; Paricaud, P., Measurements and predictive models of high-pressure H2 solubility in brine (H2O+ NaCl) for underground hydrogen storage application. *Int. J. Hydrogen Energy* **2020**.
8. Chapoy, A.; Nazeri, M.; Kapateh, M.; Burgass, R.; Coquelet, C.; Tohidi, B., Effect of impurities on thermophysical properties and phase behaviour of a CO2-rich system in CCS. *Int. J. Greenhouse Gas Control* **2013,** 19, 92-100.
9. Løvseth, S. W.; Skaugen, G.; Stang, H. J.; Jakobsen, J. P.; Wilhelmsen, Ø.; Span, R.; Wegge, R., CO2Mix Project: Experimental determination of thermo-physical properties of CO2-rich mixtures. *Energy Procedia* **2013,** 37, 7841-7849.
10. Westman, S. F.; Stang, H. J.; Løvseth, S. W.; Austegard, A.; Snustad, I.; Ertesvåg, I. S., Vapor-liquid equilibrium data for the carbon dioxide and oxygen (CO2+ O2) system at the temperatures 218, 233, 253, 273, 288 and 298 K and pressures up to 14 MPa. *Fluid Phase Equilib.* **2016,** 421, 67-87.
11. Chapoy, A.; Coquelet, C.; Burgass, R.; Tohidi, B. *Final Report JIP (confidential) : Impact of Common Impurities on CO2 Capture, Transport and Storage 2011 – 2014 PROGRAMME*; **2015**.
12. Kang, S.-P.; Lee, H.; Lee, C.-S.; Sung, W.-M., Hydrate phase equilibria of the guest mixtures containing CO2, N2 and tetrahydrofuran. *Fluid Phase Equilib.* **2001,** 185, 101-109.
13. He, J.; Liu, Y.; Ma, Z.; Deng, S.; Zhao, R.; Zhao, L., A literature research on the performance evaluation of hydrate-based CO2 capture and separation process. *Energy Procedia* **2017,** 105, 4090-4097.
14. Lunine, J. I.; Stevenson, D. J., Thermodynamics of clathrate hydrate at low and high pressures with application to the outer solar system. *Astrophys. J., Suppl. Ser.* **1985,** 58, 493-531.
15. Waals, J. v. d.; Platteeuw, J., Clathrate solutions. *Adv. Chem. Phys.* **1958**, 1-57.
16. Hajiw, M.; Boonaert, E.; Valtz, A.; El Ahmar, E.; Chapoy, A.; Coquelet, C., Impact of aromatics on acid gas injection. **2016**.
17. Tzirakis, F.; Stringari, P.; von Solms, N.; Coquelet, C.; Kontogeorgis, G., Hydrate equilibrium data for the CO2+ N2 system with the use of tetra-n-butylammonium bromide (TBAB), cyclopentane (CP) and their mixture. *Fluid Phase Equilib.* **2016,** 408, 240-247.

18. Hajiw, M. Hydrate mitigation in sour and acid gases. 2014.
19. Sloan, E.; Fleyfel, F., Hydrate dissociation enthalpy and guest size. *Fluid Phase Equilib.* **1992,** 76, 123-140.
20. Michelsen, M. L., The isothermal flash problem. Part I. Stability. *Fluid Phase Equilib.* **1982,** 9, 1-19.
21. Michelsen, M. L., The isothermal flash problem. Part II. Phase-split calculation. *Fluid Phase Equilib.* **1982,** 9, 21-40.
22. Munck, J.; Skjold-Jørgensen, S.; Rasmussen, P., Computations of the formation of gas hydrates. *Chem. Eng. Sci.* **1988,** 43, 2661-2672.
23. Parrish, W. R.; Prausnitz, J. M., Dissociation pressures of gas hydrates formed by gas mixtures. *Ind. Eng. Chem. Process Des. Dev.* **1972,** 11, 26-35.
24. Peng, D.-Y.; Robinson, D. B., A new two-constant equation of state. *Ind. Eng. Chem. Fundam.* **1976,** 15, 59-64.
25. Wertheim, M., Fluids with highly directional attractive forces. I. Statistical thermodynamics. *J. Stat. Phys.* **1984,** 35, 19-34.
26. Blum, L., Mean spherical model for asymmetric electrolytes: I. Method of solution. *Mol. Phys.* **1975,** 30, 1529-1535.
27. Born, M., Volumen und hydratationswärme der ionen. *Z. Phys.* **1920,** 1, 45-48.
28. Kontogeorgis, G. M.; Folas, G. K.; Muro-Suñé, N.; Roca Leon, F.; Michelsen, M. L., Solvation Phenomena in Association Theories with Applications to Oil & Gas and Chemical Industries. *Oil Gas Sci. Technol.* **2008,** 63, 305-319.
29. Lasala, S.; Chiesa, P.; Privat, R.; Jaubert, J.-N., VLE properties of CO2–Based binary systems containing N2, O2 and Ar: Experimental measurements and modelling results with advanced cubic equations of state. *Fluid Phase Equilib.* **2016,** 428, 18-31.
30. Dicko, M.; Coquelet, C., Application of a new crossover treatment to a generalized cubic equation of state. *Fluid Phase Equilib.* **2011,** 302, 241-248.
31. Janeček, J.; Paricaud, P.; Dicko, M.; Coquelet, C., A generalized Kiselev crossover approach applied to Soave–Redlich–Kwong equation of state. *Fluid Phase Equilib.* **2015,** 401, 16-26.
32. Kihara, T., Determination of Intermolecular Forces from the Equation of State of Gases. II. *J. Phys. Soc. Jpn.* **1951,** 6, 184-188.
33. McKoy, V.; Sinanoğlu, O., Theory of dissociation pressures of some gas hydrates. *J. Chem. Phys.* **1963,** 38, 2946-2956.
34. Hubert, N.; Gabes, Y.; Bourdet, J.-B.; Schuffenecker, L., Vapor pressure measurements with a nonisothermal static method between 293.15 and 363.15 K for electrolyte solutions. Application to the H2O+ NaCl system. *J. Chem. Eng. Data* **1995,** 40, 891-894.
35. Hamer, W. J.; Wu, Y. C., Osmotic coefficients and mean activity coefficients of uni - univalent electrolytes in water at 25° C. *J. Phys. Chem. Ref. Data* **1972,** 1, 1047-1100.
36. Rard, J. A.; Archer, D. G., Isopiestic Investigation of the Osmotic and Activity Coefficients of Aqueous NaBr and the Solubility of NaBr. cntdot. 2H2O (cr) at 298.15 K: Thermodynamic Properties of the NaBr+ H2O System over Wide Ranges of Temperature and Pressure. *J. Chem. Eng. Data* **1995,** 40, 170-185.
37. llmari Partanen, J.; Minkkinen, P. O., Thermodynamic Activity Quantities in Aqueous Sodium and Potassium Chloride Solutions at 298.15 K up to a Molality of 2.0 mol kg _1. *Acta Chem. Scand.* **1993,** 47, 768-776.
38. Robinson, R. A.; Stokes, R. H., Tables of osmotic and activity coefficients of electrolytes in aqueous solution at 25 C. *Trans. Faraday Society* **1949,** 45, 612-624.

39. Gibbard Jr, H. F.; Scatchard, G.; Rousseau, R. A.; Creek, J. L., Liquid-vapor equilibrium of aqueous sodium chloride, from 298 to 373. deg. K and from 1 to 6 mol kg-1, and related properties. *J. Chem. Eng. Data* **1974,** 19, 281-288.
40. Pitzer, K. S.; Peiper, J. C.; Busey, R., Thermodynamic properties of aqueous sodium chloride solutions. *J. Phys. Chem. Ref. Data* **1984,** 13, 1-102.
41. Guo, H.; Huang, Y.; Chen, Y.; Zhou, Q., Quantitative Raman Spectroscopic Measurements of CO2 Solubility in NaCl Solution from (273.15 to 473.15) K at p=(10.0, 20.0, 30.0, and 40.0) MPa. *J. Chem. Eng. Data* **2015,** 61, 466-474.
42. Koschel, D.; Coxam, J.-Y.; Rodier, L.; Majer, V., Enthalpy and solubility data of CO 2 in water and NaCl (aq) at conditions of interest for geological sequestration. *Fluid Phase Equilib.* **2006,** 247, 107-120.
43. Yan, W.; Huang, S.; Stenby, E. H., Measurement and modeling of CO2 solubility in NaCl brine and CO2–saturated NaCl brine density. *Int. J. Greenhouse Gas Control* **2011,** 5, 1460-1477.
44. Messabeb, H.; Contamine, F. o.; Cézac, P.; Serin, J. P.; Gaucher, E. C., Experimental Measurement of CO2 Solubility in Aqueous NaCl Solution at Temperature from 323.15 to 423.15 K and Pressure of up to 20 MPa. *J. Chem. Eng. Data* **2016,** 61, 3573-3584.
45. Ahmadi, P.; Chapoy, A., CO2 solubility in formation water under sequestration conditions. *Fluid Phase Equilib.* **2018,** 463, 80-90.
46. Bamberger, A.; Sieder, G.; Maurer, G., High-pressure (vapor+ liquid) equilibrium in binary mixtures of (carbon dioxide+ water or acetic acid) at temperatures from 313 to 353 K. *J. Supercrit. Fluids* **2000,** 17, 97-110.
47. Hou, S.-X.; Maitland, G. C.; Trusler, J. M., Measurement and modeling of the phase behavior of the (carbon dioxide+ water) mixture at temperatures from 298.15 K to 448.15 K. *J. Supercrit. Fluids* **2013,** 73, 87-96.
48. Dohrn, R.; Bünz, A.; Devlieghere, F.; Thelen, D., Experimental measurements of phase equilibria for ternary and quaternary systems of glucose, water, CO2 and ethanol with a novel apparatus. *Fluid Phase Equilib.* **1993,** 83, 149-158.
49. Wiebe, R.; Gaddy, V., The solubility in water of carbon dioxide at 50, 75 and 100, at pressures to 700 atmospheres. *J. Am. Chem. Soc.* **1939,** 61, 315-318.
50. Briones, J.; Mullins, J.; Thies, M.; Kim, B.-U., Ternary phase equilibria for acetic acid-water mixtures with supercritical carbon dioxide. *Fluid Phase Equilib.* **1987,** 36, 235-246.
51. King Jr, A. D.; Coan, C., Solubility of water in compressed carbon dioxide, nitrous oxide, and ethane. Evidence for hydration of carbon dioxide and nitrous oxide in the gas phase. *J. Am. Chem. Soc.* **1971,** 93, 1857-1862.
52. Jackson, K.; Bowman, L. E.; Fulton, J. L., Water solubility measurements in supercritical fluids and high-pressure liquids using near-infrared spectroscopy. *Anal. Chem.* **1995,** 67, 2368-2372.
53. Müller, G.; Bender, E.; Maurer, G., Das Dampf ‐ Flüssigkeitsgleichgewicht des ternären Systems Ammoniak ‐ Kohlendioxid ‐ Wasser bei hohen Wassergehalten im Bereich zwischen 373 und 473 Kelvin. *Berichte der Bunsengesellschaft für physikalische Chemie* **1988,** 92, 148-160.
54. Wylie, R. G.; Fisher, R. S., Molecular interaction of water vapor and oxygen. *J. Chem. Eng. Data* **1996,** 41, 175-180.
55. Koh, C. A.; Sloan, E. D.; Sum, A. K.; Wu, D. T., Fundamentals and applications of gas hydrates. *Annu. Rev. Chem. Biomol. Eng.* **2011,** 2, 237-257.
56. Davidson, D.; Handa, Y.; Ratcliffe, C.; Ripmeester, J.; Tse, J.; Dahn, J.; Lee, F.; Calvert, L., Crystallographic studies of clathrate hydrates. Part I. *Mol. Cryst. Liq. Cryst.* **1986,** 141, 141-149.

57. Tse, J.; Handa, Y.; Ratcliffe, C.; Powell, B., Structure of oxygen clathrate hydrate by neutron powder diffraction. *J. Inclusion Phenom.* **1986,** 4, 235-240.
58. Mohammadi, A. H.; Tohidi, B.; Burgass, R. W., Equilibrium data and thermodynamic modeling of nitrogen, oxygen, and air clathrate hydrates. *J. Chem. Eng. Data* **2003,** 48, 612-616.
59. Kezibri, N.; Bouallou, C., Conceptual design and modelling of an industrial scale power to gas-oxy-combustion power plant. *Int. J. Hydrogen Energy* **2017,** 42, 19411-19419.

TOC graph

1. Measurements

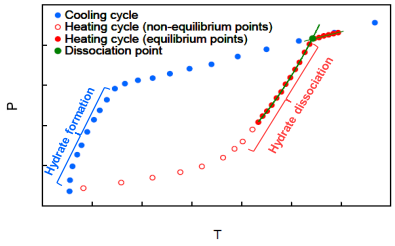

Mixed-gas hydrate study

Data processing

Predicting phase diagram

3. Applied Knowledge

- Flow assurance
- Separation process
- Underground gas storage
- Gas hydrate in the solar system

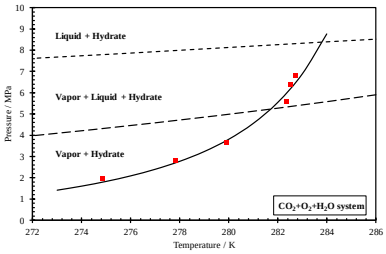

2. Modeling